Journal of Controlled Release 346 (2022) 240–249

Contents lists available at ScienceDirect

Journal of Controlled Release

journal homepage: www.elsevier.com/locate/jconrel

^{131}I-αPD-L1 immobilized by bacterial cellulose for enhanced radio-immunotherapy of cancer

Zhongyuan Qi [a,1], Pei Pei [a,1], Yanxiang Zhang [a], Hua Chen [a], Sai Yang [a], Teng Liu [a,*], Yujuan Zhang [b,*], Kai Yang [a,*]

[a] State Key Laboratory of Radiation Medicine and Protection, School of Radiation Medicine and Protection & School for Radiological and Interdisciplinary Sciences (RAD-X), Collaborative Innovation Center of Radiation Medicine of Jiangsu Higher Education Institutions, Soochow University, Suzhou, Jiangsu 215123, China
[b] Experimental Center of Suzhou Medical College of Soochow University, Suzhou, Jiangsu 215123, China

ARTICLE INFO

Keywords:
Bacterial cellulose
Immune-stimulatory
αPD-L1
Immune checkpoint blockade
Radio-immunotherapy

ABSTRACT

Radioisotope therapy (RIT) of cancer is restrained by the nonspecific distribution of radioisotope and ineptitude for metastatic tumors. Meanwhile, the clinical application of immune checkpoint blockade (ICB) confronts problems such as low responsive rate, multiple administration requirements and immune-related adverse events (irAE). To address these challenges, we prepared an injectable suspension by immobilizing ^{131}I-labeled anti-programmed cell death-ligand 1 antibody (αPD-L1) in bacterial cellulose for precise and durable radio-immunotherapy of cancer. The crisscross network structure of bacterial cellulose nanofibers would contribute to the long-term retention of ^{131}I-labeled αPD-L1 within tumors, which could reduce the side effect stemmed from the nonspecific ^{131}I distribution in normal tissues. The potent long-term RIT of ^{131}I, combined with ICB by αPD-L1, could effectively restrain the growth of primary tumor in mice. In addition to the direct killing effect, ^{131}I-αPD-L1 immobilized by bacterial cellulose could enhance the immunogenic cell death (ICD) of cancer cells, activating the maturation of multiple immune cells to induce a systemic anti-tumor immune effect. Our therapeutic strategy could suppress spontaneous cancer metastasis and prolong the survival time of tumor-bearing mice. This study proposed a new approach for combined radio-immunotherapy and a novel solution for tumor metastasis in advanced-stage cancers.

1. Introduction

Radiation therapy (RT), including external beam radiotherapy (EBRT) and internal radioisotope therapy (RIT), has been an indispensable strategy in clinical cancer treatment [1,2]. Among them, internal RIT aimed at achieving selective delivery of radiation to tumors was hampered by the nonspecific distribution and poor tumor retention of radioisotopes, which would induce unnecessary systematic toxicity and dissatisfactory therapeutic efficacy [3–5]. Meanwhile, due to the restrained effective range of radioisotope radiation, the locally applied RIT is limited for primary tumors with finite size but has little effect on late-stage tumors and cancer metastasis [6,7]. Fortunately, recent studies discovered that RT could induce immunogenic cell death (ICD) generating tumor-associated antigens (TAAs) to trigger immune response, providing a powerful support for radio-immunotherapy of cancer [8–10]. However, there have been reports showing that RIT would promote the expression of programmed cell death-ligand 1 (PD-L1) on cancer cells, which largely inhibits the $CD8^+$ T cell-dependent cellular immune process and thus undermine anti-tumor immune responses [11–13].

Immune checkpoint blockade (ICB) therapy based on monoclonal antibody could reactivate the antitumor immune response by disrupting co-inhibitory T cell signaling, which has achieved delightful clinical effects on several kinds of tumors [14–17]. Nevertheless, the generalized clinical application of ICB confronts problems such as low responsive rate, multiple administration requirements and immune-related adverse events (irAE) [18–21]. Hence, it would be a complementary cancer therapy strategy to combine RIT and ICB, among which RIT treats the primary tumor and induce ICD to promote the tumor immunogenicity, while ICB prevents PD-L1 from binding with PD-1 to inhibit the immune evasion effect [22,23]. Typically, atezolizumab is a US Food and Drug Administration (FDA)-approved monoclonal antibody (mAb) inhibitor

* Corresponding author.
E-mail addresses: tliu13@suda.edu.cn (T. Liu), zhangyujuan@suda.edu.cn (Y. Zhang), kyang@suda.edu.cn (K. Yang).
[1] Contributed equally to this work.

https://doi.org/10.1016/j.jconrel.2022.04.029
Received 24 January 2022; Received in revised form 26 March 2022; Accepted 17 April 2022
Available online 26 April 2022
0168-3659/© 2022 Elsevier B.V. All rights reserved.

for ICB [24], which could also be labeled with radioisotopes for SPECT/CT imaging [25]. Therefore, with the help of suitable biomedical scaffold, αPD-L1 would be an ideal agent for precise and durable radio-immunotherapy of cancer.

Cellulose is the most available polymer in the world, which has been traditionally extracted from plants and the derivatives [26,27]. In 1988, Brown discovered that the fermentation of bacteria, such as *Acetobacter xylinum*, could produce bacterial cellulose (BC) with similar chemical structure and nanostructure to that of plant cellulose (PC) [28–32]. However, different from PC, BC possesses pure glucose monomer with high polymerization degree and crisscross network structure, leading to fascinating properties such as better water holding capacity, higher mechanical strength and better biocompatibility [33], which are beneficial for long-term retention of therapeutic agents in body. Moreover, the most significant difference of BC from PC is the presence of the lipopolysaccharide (LPS), an outer membrane component of Gram-negative bacteria such as *Acetobacter xylinum*. Composed of lipids and polysaccharides with abundant hydroxyl groups and some amide group, LPS may induce serious inflammatory responses in a large dose [34]. Meanwhile, a low dose of LPS is expected to be an ideal stimulant for immunologic priming [35–37], making BC a promising biomedical scaffold for the local administration of therapeutic agents for enhanced radio-immunotherapy. So far, several methods for immobilization of radionuclides or macromolecules *in situ* have been reported, such as hydrogels or microspheres [38–41]. Such methods can only trap the radionuclides in place, yet the immunosuppression caused by radiation remain unsolved. As a comparison, BC can induce an immune activating effect through LPS, enhancing the immune function to generate a synergistic therapeutic effect, which is superior to other methods.

Herein, we developed an injectable suspension by immobilizing ^{131}I-labeled atezolizumab in BC (^{131}I-αPD-L1/BC) to achieve precise and durable radio-immunotherapy of cancer. Taking advantage of the excellent network structure of BC nanofibers, ^{131}I-labeled αPD-L1 could stay in the tumor sites for a long period after intratumoral injection. In addition to the long-term immobilization effect for local RIT, ^{131}I-αPD-L1/BC could also function as an effective immune activator. RIT-induced ICD could generate TAAs from dead cancer cells and activate multiple immune cells. Notably, the radiation-induced increase of PD-L1 expression on tumor cells could be counteracted by the local administration of αPD-L1. Moreover, BC itself is a safe and potent source of immune stimulation, whose LPS at a relatively low dose could evidently activate the immune response. Furthermore, the powerful stimulating effect on dendritic cells (DCs) maturation and the higher ratio of CD8$^+$ CTL tumor infiltration induced by our treatment provided support for spontaneously metastatic tumor inhibition. Therefore, a biocompatible suspension containing BC and ^{131}I-αPD-L1 was developed by a simple mixing approach to achieve enhanced radio-immunotherapy in a synergetic manner (Fig. 1), exhibiting extraordinary potential for clinical translation.

2. Materials and methods

2.1. Materials

Acetobacter xylinum was obtained from BNCC (BeNa Culture Collection). Plant cellulose was purchased from Sanjia. Cellulase was purchased from Macklin. ^{131}I was purchased from Shanghai GMS Pharmaceutical Co., Ltd. Anti-PD-L1 antibodies were purchased from Bioxcell (Clone: 10F.9G2, Catalog#: BE0101). Antibodies for γ-H2AX or PD-L1 immunofluorescence assay and flow cytometry assays were obtained from eBioscience. The ELISA kits for LPS assay were purchased from Sanjia. The ELISA kits for TNF-α and IFN-γ measurement were purchased from Dakewe Biotech. CT26 colon cancer cells and 4 T1 breast cancer cells were originally obtained from Cell Source Center, Chinese Academy of Science (Shanghai, China).

2.2. ^{131}I labeling of αPD-L1

αPD-L1 was labeled with radionuclide ^{131}I through a standard iodogen oxidation method [42]. In brief, 1 mL of iodogen dissolved in dichloromethane (1 mg ml^{-1}) was added into a 2 ml eppendorf tube and then blown-dried with nitrogen. Afterwards, 2 mCi of ^{131}I and 160 μL of αPD-L1 solution (6.324 μg μl^{-1}) were mixed, and the mixture was reacted for 15 min at room temperature. Excess ^{131}I was removed by ultrafiltration centrifugal filters (10 kDa) and washed several times with PBS (pH 7.2). For radiolabeling stability measurement, ^{131}I-αPD-L1 was dissolved in PBS and filtered through ultrafiltration every 24 h. The retained radioactivity was detected by gamma counter (PerkinElmer) to evaluate the radiolabeling stability.

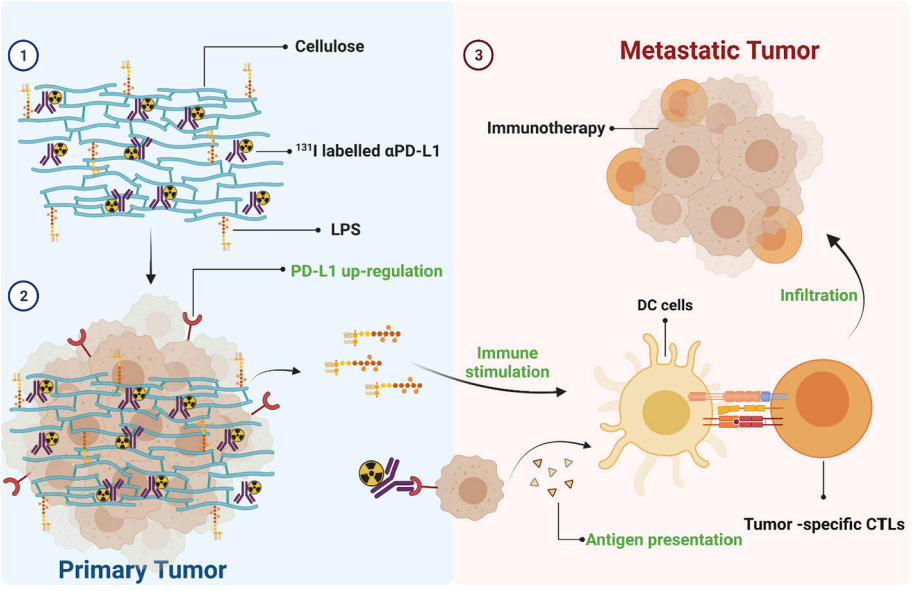

Fig. 1. Schematic diagram of ^{131}I-αPD-L1/BC for enhanced radio-immunotherapy. Schematic illustration of the antitumor immune responses induced by combining radioisotope therapy and immune checkpoint blockade on the basis of ^{131}I-αPD-L1/BC.

2.3. Preparation of cellulose suspension

Acetobacter xylinum was cultured in a fermentation medium containing yeast extract (15 mg ml^{-1}), glucose (50 mg ml^{-1}) and $CaCO_3$ (1 mg ml^{-1}) in a flask for 2 weeks until the formation of cellulose film floating on the surface of culture medium. The cellulose film was collected and soaked in 0.4% acetic acid overnight and then boiled in 4% NaOH for 2 h to remove residual culture medium. Afterwards, the bacterial cellulose film was freeze-dried and stored at room temperature.

To prepare the cellulose suspension, 50 mg of plant cellulose or freeze-dried bacterial cellulose were cut into pieces, and then mixed with 2 ml cellulase (10 mg ml^{-1}). After 4 h of incubation at room temperature, the sample was centrifuged at 4000 r/min to remove excess cellulase and washed several times with water.

2.4. Cellular experiments

CT26 colon cancer cells and 4 T1 breast cancer cells were cultured in DMEM-high glucose supplemented with 10% fetal bovine serum (FBS) and 1% penicillin–streptomycin in a humidified atmosphere containing 5% CO_2 at 37 °C. For *in vitro* cytotoxicity assay, CT26 cells and 4 T1 cells were firstly seeded into 96-well plates at a density of 8000 cells per well for 24 h and then incubated with different concentrations of bacteria cellulose, ^{131}I-αPD-L1 or free ^{131}I for 24 h. Relative cell viabilities were then evaluated *via* cell counting kit-8 (CCK-8) assay.

2.5. Tumor model

Female BALB/c mice (6–8 weeks) were purchased from Changzhou Kavins Experimental Animal Co., Ltd. Animal experiments were strictly performed according to protocols approved by Soochow University Laboratory Animal Center. To establish the bilateral tumor model, 50 μL PBS containing the same number of CT26 (or 4 T1) cells (2×10^6) was injected into both flanks of the back of mice at the same day. The imaging of mice was conducted by a small animal SPECT/CT imaging system (U-SPECT+/CT, MILabs Corporation) at different time points including 2, 8, 24 and 48 h post i.t. injection. To investigate the biodistribution of ^{131}I-αPD-L1, CT26 tumor-bearing BALB/c mice were i.t. injected with ^{131}I-αPD-L1, ^{131}I-αPD-L1/BC, ^{131}I-αPD-L1/PC or free ^{131}I, respectively. Afterwards, the major tissues including liver, spleen, kidney, heart, lung and tumor were collected for gamma counter measurement.

To establish spontaneous metastatic 4 T1 orthotopic murine breast cancer model, fLuc-4 T1 cells (5×10^5) dispersed in PBS were injected into the right-side breast pad of each mouse. After 15 days, mice were randomly divided into 4 groups, and intratumorally injected with ^{131}I-αPD-L1, ^{131}I-αPD-L1/BC (BC, 500 μg), ^{131}I-αPD-L1/PC (PC, 500 μg) or PBS, respectively (dose of ^{131}I = 50 μCi per mouse, dose of αPD-L1 = 25 μg per mouse). 5 days after the injection, the tumors of mice in ^{131}I-αPD-L1/BC treated group were cured by radio-immunotherapy, while the tumors of the mice in other groups were surgically removed. Spontaneous metastases of tumor cells were monitored by an IVIS spectrum imaging system from day 0 to day 15.

2.6. Radio-immunotherapy

CT26 or 4 T1 tumors were inoculated into both flanks of all mice back. When both tumors reached 75 mm^3, mice were randomly divided into 7 groups ($n = 5$ per group). Mice were intratumorally (i.t.) injected to the right flank tumor with plant cellulose (PC) (500 μg), BC (500 μg), ^{131}I-αPD-L1, ^{131}I-αPD-L1/BC (BC, 500 μg), ^{131}I-αPD-L1/PC (PC, 500 μg), free ^{131}I or PBS at day 0 (dose of ^{131}I = 50 μCi per mouse, dose of αPD-L1 = 25 μg per mouse), and the left flank tumor will be taken as distal tumors. BC and PC were both digested into an injectable fluid by cellulase before injection. Afterwards, the tumor volumes were monitored with a vernier caliper every 2 days and calculated by the following formula: volume = (tumor length) × (tumor width)^2/2. Mice were euthanized upon the volume of tumors reached 1000 mm^3.

2.7. Ex vivo analysis of PD-L1 expression on tumor cells

To study the PD-L1 expression caused by radiation on tumor cells, CT26 tumors were collected from mice by surgery and homogenized in PBS (pH 7.4) containing 1% fetal bovine serum (FBS). For immunofluorescence staining, tumor slices were stained with DAPI and αPD-L1-FITC (Abcam, [EPR20529], ab213480).

2.8. Ex vivo analysis of dendritic cells

To explore *in vivo* DCs maturation studies, the lymph gland was obtained from the ipsilateral inguinal of each CT26 tumor-bearing mouse 3 days post treatments (PC, BC, ^{131}I-αPD-L1, ^{131}I-αPD-L1/BC, ^{131}I-αPD-L1/PC, free ^{131}I or PBS) and homogenized in PBS (pH 7.4) containing 1% FBS to prepare a cell suspension. After that, the DCs were stained with anti-CD11c-FITC (eBioscience, Clone: N418, 11–0114-82), anti-CD86-APC (eBioscience, Clone: GL1, 17–0862-82) and anti-CD80-PE (eBioscience, Clone: 16-10A1, 12–0801-82) antibodies for flow cytometry assays.

2.9. Ex vivo analysis of T cells

To evaluate immune cell infiltration in tumors, both primary and distal tumors from mice after different treatments were collected and then cut into pieces to obtain a single-cell suspension. The samples were then stained with the corresponding antibodies according to our previous study [22,43]. In brief, cancer cells were stained with anti-CD3-FITC (eBioscience, Clone: 17A2, 11–0032-82), anti-CD8a-PE (eBioscience, Clone: 53–6.7, 12–0081-83) and anti-CD4-APC (eBioscience, Clone: GK1.5, 17–0041-83) antibodies to distinguish cytotoxic T lymphocytes ($CD3^+CD4^+CD8^-$) and helper T cells ($CD3^+CD4^+CD8^-$).

2.10. Cytokine detection

Serum samples were isolated from mice after different treatments and diluted for analysis. TNF-α and IFN-γ were analyzed by the corresponding ELISA kits according to the vendors' protocols.

3. Results and discussion

Bacterial cellulose (BC) is an extracellular metabolic product of *Acetobacter xylinum*. After static cultivation of *Acetobacter xylinum* in a specific fermentation medium for two weeks, a layer of BC film was formed floating on the surface of culture medium (**Supporting information Fig. S1**) [44]. After collection and freeze-drying, the natural BC film was cut into small pieces and then digested by cellulase, turning into BC suspension (**Supporting information Fig. S2**). Subsequently, the rheological properties of BC before and after digestion by cellulase were tested by rheometer. The cellulase-digested BC demonstrated an obvious attenuation in both storage modulus (G′) and loss modulus (G") (Supporting information Fig. S3), suggesting that the cellulase-digested BC suspension has relatively weaker mechanical strength and more fluid-like behavior, which is suitable for medical injection. Since the crisscrossed joints between cellulose nanofibers were cut by cellulase, BC exhibited a more loosened structure than natural BC (Fig. 2a**, Supporting information Fig. S4**).

In order to identify the difference in chemical groups, Fourier transform infrared spectroscopy (FT-IR) was conducted to characterize the BC and plant cellulose (PC). The FT-IR spectra of BC and PC demonstrated similar broad peaks around 3327 cm^{-1} and sharp peaks at 2904 cm^{-1}, which were respectively corresponding to the stretching vibration of -OH and C—H groups in polysaccharides [45,46]. Meanwhile, the FT-IR spectrum of BC demonstrated more sharp vibrational

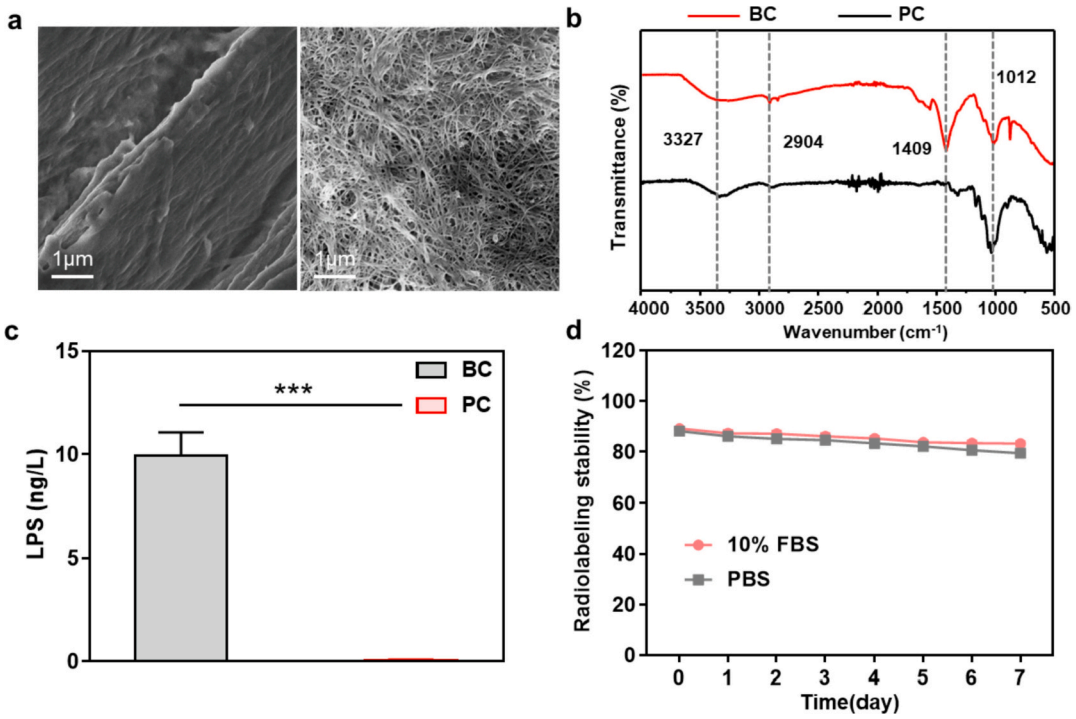

Fig. 2. Characterization of bacterial cellulose. (a) SEM images of natural BC (left) and cellulase-digested BC (right). **(b)** FT-IR spectra of BC and PC. **(c)** LPS concentration in BC and PC suspension. *P* value was calculated by multiple *t*-tests (***$P < 0.001$). **(d)** Radiolabeling stability of ^{131}I-αPD-L1/BC in PBS with or without serum.

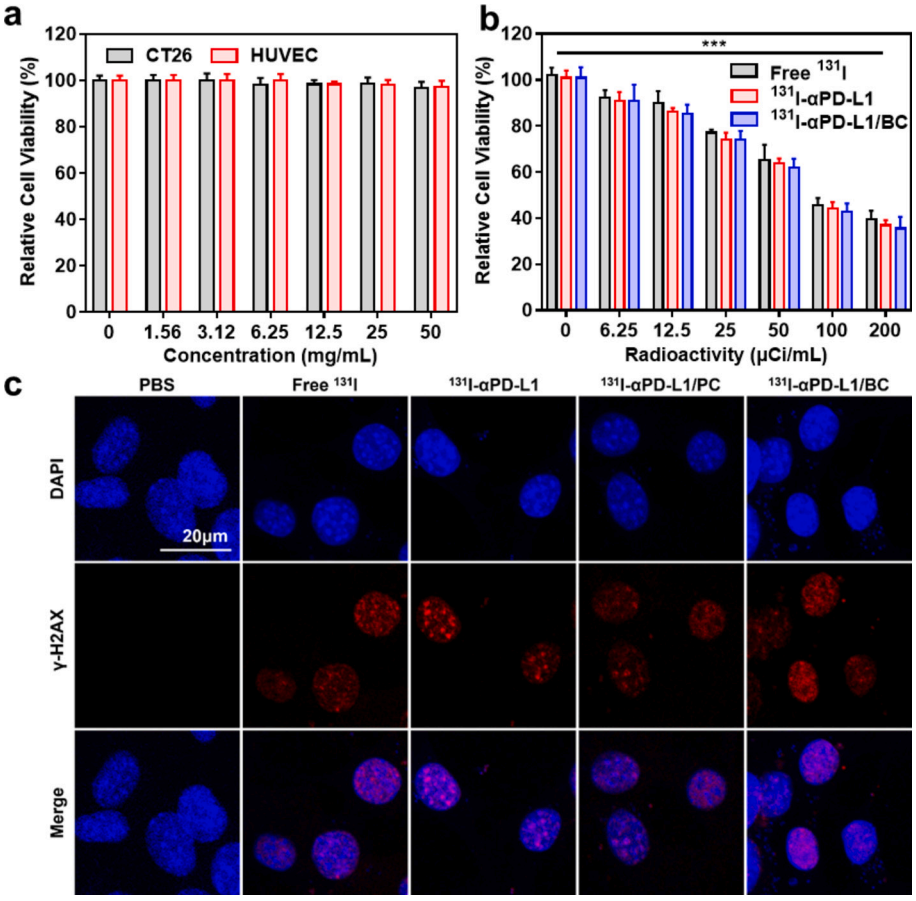

Fig. 3. Cellular experiments. (a) Relative viabilities of HUVEC and CT26 cells after incubation with BC at different concentrations for 24 h. **(b)** Relative viabilities of CT26 cells after incubation with free ^{131}I, ^{131}I-αPD-L1 and ^{131}I-αPD-L1/BC at different doses for 72 h. *P* values were calculated by multiple t-tests (***$P < 0.001$). **(c)** Confocal imaging of CT26 cells at 24 h post different treatments (blue: DAPI, red: γ-H2AX). (For interpretation of the references to colour in this figure legend, the reader is referred to the web version of this article.)

bands compared to PC, with the most significant peak at 1627 and 1405 cm^{-1} assigned to the vibrational modes (antisymmetric and symmetric stretching, respectively) of -COO groups, which were especially existing in LPS (Fig. 2b) [47]. To further verify the unique presence of LPS in BC, the LPS concentration in both cellulose solutions was quantified by ELISA kits (Fig. 2c), showing negligible LPS in PC while 9.9 ng/L of LPS in BC solution, indicating the specific function of BC for stimulating immune response.

Owing to the appropriate β (99%) and γ (1%) emission intensity, ^{131}I has been widely used for the theranostics of thyroid disease in clinic. The energy of β particles emitted by ^{131}I is up to 0.6 MeV, which has a strong killing effect on cancer cells. Due to the half-life of 8.03 days, ^{131}I could provide enough activity even after a week. Importantly, compared with the other radioisotopes such ^{177}Lu and ^{188}Re, ^{131}I is relatively cheap and easily available. FDA-approved PD-L1 inhibitor atezolizumab with tyrosine-rich structure has been utilized for ICB treatment. Herein, atezolizumab was labeled with ^{131}I by the substitution reaction on the tyrosine, obtaining ^{131}I-αPD-L1 with a high radiolabeling yield (86.5 ± 3%) and excellent radiolabeling stability in both 10% FBS and PBS even after seven days (Fig. 2d). Additionally, the bioactivity of ^{131}I labeled αPD-L1 was tested. In brief, CT26 cells were incubated with αPD-L1 and ^{131}I-αPD-L1 respectively for flow cytometry assay. αPD-L1 and ^{131}I-αPD-L1 exhibited similar binding efficacy to PD-L1 on CT26 cells, indicating that the^{131}I labeling would not affect the bioactivity of αPD-L1 (**Supporting information Fig. S5**). Afterwards, ^{131}I-αPD-L1 was immobilized into BC matrix by simply mixing, achieving ^{131}I-αPD-L1/BC for the subsequent experiments.

The cytotoxicity of BC and ^{131}I-labeled αPD-L1/BC was investigated in both CT26 (murine colon cancer cells) and HUVECs (human umbilical vein endothelial cells). The cellular viability was tested by cell counting kit-8 (CCK-8) assay after incubation with BC at different concentrations for 72 h. BC showed negligible influence on the viability of both cell lines even at the highest concentration (50 mg ml^{-1}), indicating the superior biocompatibility *in vitro* (Fig. 3a). Meanwhile, free ^{131}I, ^{131}I-αPD-L1 and ^{131}I-αPD-L1/BC exhibited similar toxicity to CT26 cells, suggesting that the direct cell death was mainly derived from RIT by therapeutic radioisotope ^{131}I, and BC would not affect the killing effect of ^{131}I (Fig. 3b). The DNA double-strand breaks of CT26 cells after ^{131}I-αPD-L1/BC incubation was then evaluated by γ-H2AX, a commonly used marker for DNA breaks. The confocal imaging of cells treated with ^{131}I-αPD-L1/BC, similar to ^{131}I or ^{131}I-αPD-L1 treated cells, illustrated obvious red fluorescence for DNA double-strand breaks (Fig. 3c), validating that BC would not compromise the powerful RIT efficacy to cancer cells.

Encouraged by the biocompatibility of BC and efficient RIT of ^{131}I-αPD-L1/BC *in vitro*, the influence of ^{131}I-αPD-L1/BC on immune response *in vivo* was then evaluated. The expression of PD-L1 in CT26 tumors was tested 72 h post intratumoral (i.t.) injection of free ^{131}I or ^{131}I-αPD-L1 to assess the immunoregulatory activity (Fig. 4a&b). Compared to the control group, the immunofluorescence-stained tumor slice demonstrated slightly stronger PD-L1 fluorescence (green) in those treated with ^{131}I, which was in consistent with previous studies reporting that radiation exposure would up-regulate the PD-L1 expression in tumor cells. Interestingly, the tumor treated with ^{131}I-αPD-L1 showed less PD-L1 signal as compared to free ^{131}I, validating the successful interaction of αPD-L1 with PD-L1. The immunofluorescent images of tumors together indicated the efficacy of ^{131}I-αPD-L1 to block RIT-induced PD-L1 expression and the possibility for combined RIT and immunotherapy.

Dendritic cells (DCs), as a representative kind of antigen-presenting cells (APCs) to activate T cells, play a pivotal role in triggering and regulating immune responses only upon maturation [48,49]. In order to

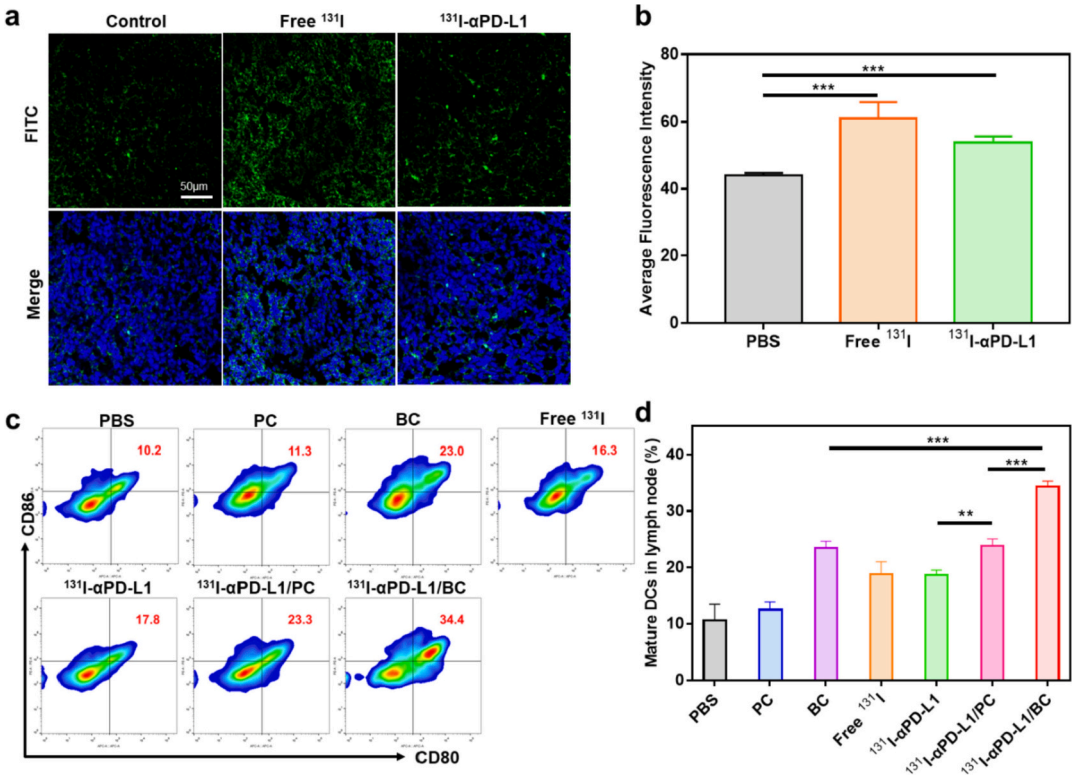

Fig. 4. Immunostimulatory effects of ^{131}I-αPD-L1/BC *in vivo*. (a, b) Immunofluorescence-stained tumoral slices illustrating the PD-L1 expression **(a)** and the corresponding statistical data of average fluorescence intensity **(b)** (blue: DAPI, green: PD-L1). **(c, d)** Flow cytometry results showing the DC maturation proportions in CT26 tumor-bearing mice **(c)** and the corresponding statistical plots **(d)**. Lymph node cells were harvested 3 days after treatments and stained with CD11c, CD80 and CD86 for flow cytometry experiments. Error bars represent mean ± s.d. ($n = 5$). P values in **b&d** were calculated by multiple t-tests (***P < 0.001, **$P < 0.01$, *$P < 0.05$). (For interpretation of the references to colour in this figure legend, the reader is referred to the web version of this article.)

study the DC maturation ratio after various treatments, the lymph gland was then collected from the ipsilateral inguinal of each CT26 tumor-bearing mouse and analyzed by flow cytometry (Fig. 4c&d). Free ^{131}I itself, as well as ^{131}I-αPD-L1, could slightly elevate the ratio of DC maturation, verifying the stimulating efficacy of RIT. Since PC showed limited influence on DC maturation as compared to PBS, more DC maturation in ^{131}I-αPD-L1/PC treated group than those in ^{131}I-αPD-L1 group was reasonable ascribed to the retention of ^{131}I-αPD-L1 in the tumor site by PC. Encouragingly, due to the synergistic stimulation effect of RIT and LPS as well as the immobilization capability of BC, ^{131}I-αPD-L1/BC group showed the most significant DC maturation, indicating the promise of ^{131}I-αPD-L1/BC as an immune stimulant to initiate and reinforce immune responses. Interestingly, BC alone obviously enhanced DC maturation. Thus, to investigate the mechanism of the immune stimulating effect of BC, the DC maturation ratio of mice treated with BC or PC added with the same amount of LPS (9.9 ng/L) was tested by flow cytometry (**Supporting information Fig. S6**). Both of BC and PC + LPS could effectively stimulate the DC maturation, and there was no significant difference between each other. Such results further verified that the immune activating effect of BC was attributed to LPS.

Before application for cancer radio-immunotherapy, the biodistribution of radionuclides in tumor-bearing mice was evaluated by SPECT/CT imaging after i.t. injection of ^{131}I-αPD-L1 (50 μCi), ^{131}I-αPD-L1/BC (50 μCi, 500 μg of BC), ^{131}I-αPD-L1/PC (50 μCi; PC, 500 μg) or free ^{131}I (50 μCi), respectively (Fig. 5a). It was found that free ^{131}I rapidly fled from tumor post injection and exhibited significant thyroid accumulation within hours, while most of ^{131}I-αPD-L1 retained in the tumor after 8 h and then gradually eliminated with certain thyroid accumulation after 48 h. In contrast, both ^{131}I-αPD-L1/BC and ^{131}I-αPD-L1/PC showed significantly long-term retention in tumor without any thyroid accumulation, which is favorable for safe and efficient RIT *in vivo*. Furthermore, the *ex vivo* distribution of ^{131}I-αPD-L1 in tumors and major organs were then statistically measured by gamma counter at 48 hand 72 h post i.t. injection (Fig. 5b&c). Compared with free ^{131}I-αPD-L1,^{131}I-αPD-L1/PC and ^{131}I-αPD-L1/BC exhibited higher radioactivity in the tumor sites at each time point, which is coincident with the SPECT/CT imaging results. Among them, due to the crisscrossed network of BC nanofibers, ^{131}I-αPD-L1/BC exhibited the strongest tumoral retention without any signal in normal organs, suggesting the capability of BC as a superior scaffold to immobilize radionucleotides and monoclonal antibodies (mAbs) for enhanced RIT and immunotherapy without the concern of unnecessary side-effect.

Encouraged by the favorable performance of BC in long-term tumor retention and stimulating DC maturation, we then evaluated the efficiency of ^{131}I-αPD-L1/BC for combined RIT and immunotherapy. In detail, a bilateral tumor model was built by inoculation of CT26 cells on both flanks of the back of BALB/c mice. When the average volume of tumors reached ~75 mm^3, the mice were randomly assigned into seven groups (n = 5 per group) including 1) PBS, 2) PC (500 μg per mouse), 3) BC (500 μg per mouse), 4) free ^{131}I (50 μCi per mouse), 5) ^{131}I-αPD-L1 (50 μCi per mouse), 6) ^{131}I-αPD-L1/PC (50 μCi of ^{131}I and 500 μg of PC per mouse) and 7) ^{131}I-αPD-L1/BC (50 μCi of ^{131}I and 500 μg of BC per mouse). The tumor in the right flank of each mouse was treated with i.t. injection (primary tumor), while the left one leaved untreated (distal tumor).

The volume of both tumors was monitored every other day (Fig. 5d&e). It was discovered that although free ^{131}I and ^{131}I-αPD-L1 could slightly restrain the tumoral volume, the growth of either primary or distal tumors was still overwhelming due to the rapid elimination of radionuclides. Meanwhile, BC alone showed slightly stronger

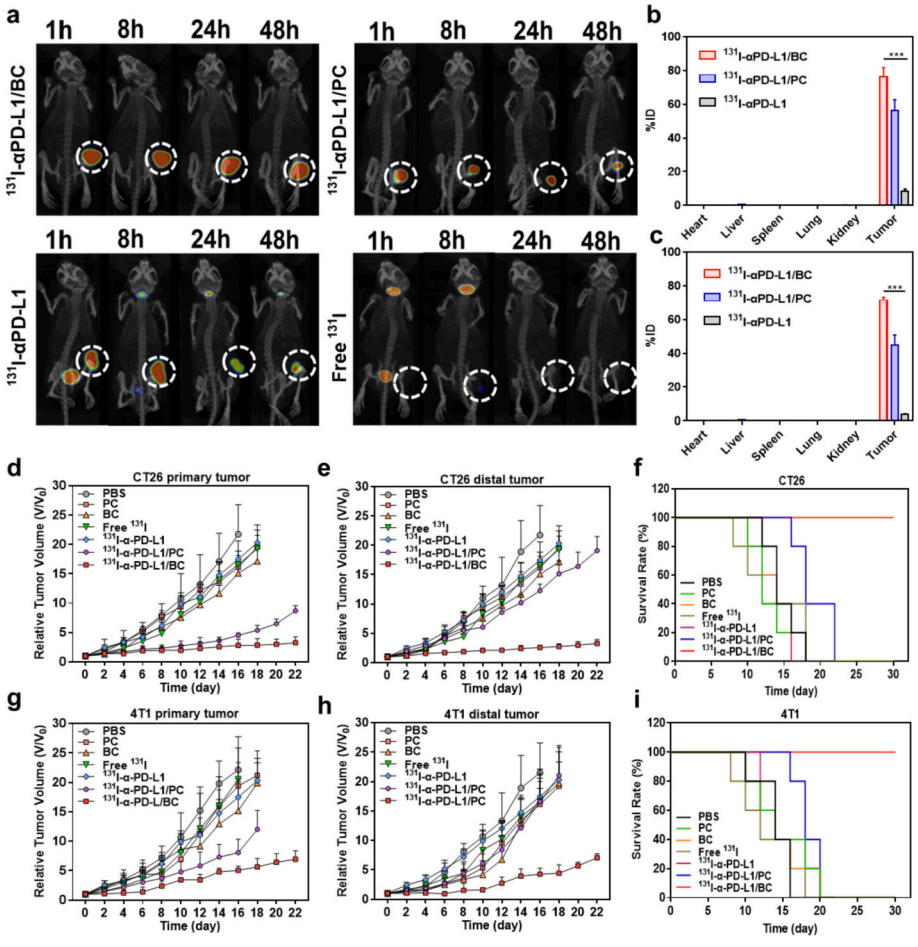

Fig. 5. Biological distribution and radio-immunotherapy of subcutaneous tumors. (a) SPECT/CT images of CT26 tumor-bearing mice at different time points after i.t. injection of ^{131}I-αPD-L1/BC, ^{131}I-αPD-L1/PC, ^{131}I-αPD-L1 or free ^{131}I, respectively. **(b, c)** Statistical biological distribution of ^{131}I-αPD-L1/BC, ^{131}I-αPD-L1/PC and ^{131}I-αPD-L1 in mice at 48 h **(b)** and 72 h **(c)** post i.t. injection. Error bars represent mean ± s.d. (n = 3). P values were calculated by multiple t-tests (***P < 0.001). **(d, e)** Tumor growth curves of local tumors **(d)** and distal tumors **(e)** in subcutaneous CT26 tumor model after different treatments. **(f)** Survival rates of CT26 tumor-bearing mice after different treatments. **(g, h)** Tumor growth curves of local tumors **(g)** and distal tumors **(h)** in 4 T1 subcutaneous tumor model after different treatments. **(i)** Survival rates of 4 T1 tumor-bearing mice after different treatments.

suppression of both tumors as compared to PC, which may be ascribed to the immune-stimulating effect of LPS. With the help of PC stabilization, ^{131}I-αPD-L1/PC effectively inhibited the growth of primary tumors in the first two weeks, while the primary tumors germinated again after 16 days, let alone distal tumors uncontrollably growing. In contrast, ^{131}I-αPD-L1/BC showed satisfactory long-term controlling over the growth of both primary and distal tumors. Correspondingly, while ^{131}I-αPD-L1/PC could only extend the life span of CT26-bearing mice from 18 days to 22 days, all the mice treated with ^{131}I-αPD-L1/BC were still alive during the observation period (Fig. 5f). The fascinating therapeutic effect of tumor by ^{131}I-αPD-L1/BC could be attributed to the BC scaffold, which could not only immobilize radionuclides and mAbs for long-term RIT and immunotherapy, but also stimulate immune response by LPS to further enhance radio-immunotherapy.

In order to evaluate the universality of ^{131}I-αPD-L1/BC for enhanced radio-immunotherapy of cancer, breast cancer model with relatively low response rate to ICB was then established by injecting 4 T1 cells into both flanks of mice. Similar to CT26 model, PC, BC, ^{131}I or ^{131}I-αPD-L1 alone showed limited effect on suppressing 4 T1 tumors on either side of mice (Fig. 5g&h). Differently, ^{131}I-αPD-L1/PC could even hardly restrain the growth of 4 T1 primary tumors in 18 days and showed negligible influence on the distal tumors. Meanwhile, mice treated with ^{131}I-αPD-L1/BC demonstrated obvious growth inhibition of both tumors and prolonged survival time over 30 days (Fig. 5i). Meanwhile, the body weight of the mice was monitored and showed no obvious change during the observation period, indicating that our strategy had no significant toxic effects on the mice (**Supporting information Fig. S7**). Altogether, ^{131}I-αPD-L1/BC exhibited encouraging therapeutic efficacy, obvious distal effect, satisfactory biosafety as well as universality in treating different tumors, preliminarily showing the promise of this strategy for clinical cancer treatment.

Moreover, the mechanism of the excellent antitumor therapeutic efficiency by ^{131}I-αPD-L1/BC was evaluated by collecting both primary and distal CT26 tumors from mice at day 5 post each treatment and testing tumor infiltrating lymphocytes (TILs) by flow cytometry (Fig. 6a-b). As for the primary tumors, those treated with BC possessed more activated CD8$^+$ cytotoxic T lymphocytes (CTLs) in TILs than those treated with PC, verifying the function of BC in activating CTLs (Fig. 6a&c). RIT, especially stabilized by PC, could elevate the ratio of CD8$^+$ CTLs to a certain extent. It's worth noting that ^{131}I-αPD-L1/BC, among all the treatments, induced the most prominent CD8$^+$ CTLs infiltrating into the primary tumors, which is in coincidence with the beast therapeutic efficacy. As for the distal tumors, the ratio of CD8$^+$ CTLs demonstrated the similar profile to that of primary tumors, showing the most significant increase of CD8$^+$ CTLs percentage in the ^{131}I-αPD-L1/BC group compared with the other groups (Fig. 6b&d). In addition, since CD3$^+$ T lymphocytes are consisted of CD4$^+$ and CD8$^+$ T cells, the increase of the proportion of CD8$^+$ cells in the ^{131}I-αPD-L1/BC treated group naturally led to the decrease of CD4$^+$ cells (**Supporting information Fig. S9**). The reduction of T-reg cells (regulatory cells) as a kind of immunosuppressive CD4$^+$ cells would also induce a positive effect on anti-tumor immunity. These results demonstrated that ^{131}I-αPD-L1/BC, taking advantage of the long-term RIT-triggered release of TAAs in combination with the strong immune stimulation effect of LPS, possessed particularly potent efficacy in activating, trafficking and infiltrating CTLs into both primary and distal tumors for robust and lasting immune response, which could preliminarily explain for its outstanding anticancer therapeutic effect. Since tumor necrosis factor alpha (TNF-α) and interferon gamma (IFN-γ) play important roles in cytotoxic effect of CTLs, the concentration of these cytokines in serum of mice was analyzed by ELISA kits at day 5 post each treatment (Fig. 6e-f). Both cytokines showed the highest concentration in mice after the radio-immunotherapy of ^{131}I-αPD-L1/BC, which further proved the robust systemic antitumor immune effect by our strategy. Results above strongly indicated that ^{131}I-αPD-L1/BC could not only kill tumors directly by radionuclide radiation, but also trigger systemic antitumor immune response to suppress the growth of tumors by distal effect.

After verifying the potent therapeutic effect and clarifying the mechanism of ^{131}I-αPD-L1/BC in treating subcutaneous tumors, an orthotopic breast tumor model was established for further evaluation of

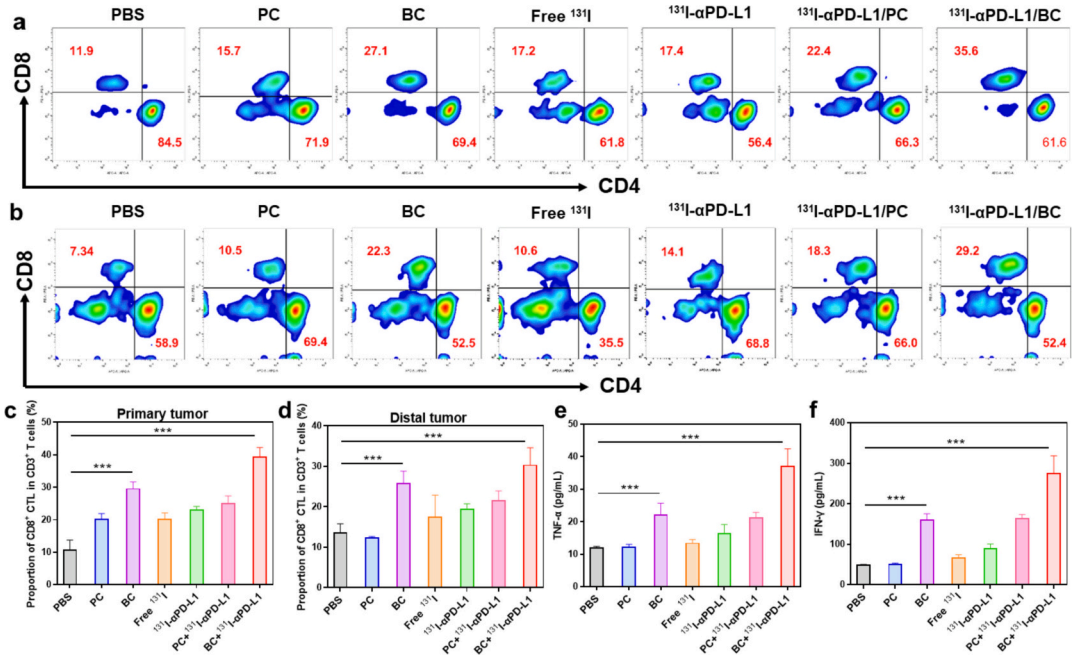

Fig. 6. Immune response post radio-immunotherapy. (a, b) Flow cytometry results showing different types of T cells in the primary tumors **(a)** and distal tumors **(b)** in different groups at 5 days post treatment (CT26 tumor model). **(c, d)** Proportions of CD8$^+$ CTLs in CD3$^+$ T cells in primary tumors **(c)** and distal tumors **(d)** after various treatments. The proportions were calculated by the following formula: Proportion = CD8$^+$ / (CD4$^+$ + CD8$^+$). The proportions were calculated by the following formula: Proportion = CD8$^+$ / (CD4$^+$ + CD8$^+$). Error bars represent mean ± s.d. (n = 5). **(e, f)** Antitumor cytokine levels including TNF-α **(e)** and IFN-γ **(f)** in serum collected from mice at 5 days after different treatments. Error bars represent mean ± s.d. (n = 5). P values were calculated by multiple t-tests (***P < 0.001).

the systemic antitumor immune response, in which 4 T1 cells expressing firefly luciferase (fLuc-4 T1) were injected into the breast pad of BALB/c mice (Fig. 7a). At 15 days post the 4 T1 inoculation, the local tumors were respectively i.t. injected with PBS, ^{131}I-αPD-L1, ^{131}I-αPD-L1/PC or ^{131}I-αPD-L1/BC. At day 5, the local tumors in the first three groups were removed by surgery, leaving those in the last group untreated. The spontaneous metastases in mice were imaged every five days by small animal fluorescent imaging system (IVIS) since the fifth day. The bioluminescence imaging demonstrated obvious cancer metastases in mice treated with PBS, ^{131}I-αPD-L1 or ^{131}I-αPD-L1/PC, resulting in all mice dead at day 15 (Fig. 7b-c). In remarkable contrast, the local treatment by ^{131}I-αPD-L1/BC not only eradicated the primary tumors at day 5, but also inhibit the cancer metastases later on, achieving 100% survival rate with steady body weight during the observation period (Fig. 7b-c, **Supporting information Fig. S10**). The success of ^{131}I-αPD-L1/BC in inhibiting spontaneous metastases suggests immobilization of therapeutic radionuclides and αPD-L1 mAbs by BC as a potential therapeutic strategy for late-stage tumors and metastases.

The high survival rate and steady body weight of mice treated with ^{131}I-αPD-L1/BC preliminarily implies the biosafety of this therapeutic strategy. In addition, the potential side-effect of ^{131}I-αPD-L1/BC was further evaluated by histological analysis. After i.t injection of ^{131}I-αPD-L1/BC (^{131}I, 50 μCi; BC, 500 μg per mouse), the mice were sacrificed at 16th day, with major organs collected for hematoxylin and eosin (H&E) staining. The H&*E*-stained slices showed negligible histopathological abnormality or damage in major organs of mice, indicating that ^{131}I-αPD-L1/BC induced no harm to the treated mice (**Supporting information Fig. S11**). Therefore, we have designed a safe and efficient strategy to treat cancer by enhanced antitumor radio-immunotherapy based on ^{131}I-αPD-L1/BC.

4. Conclusions

The application of radionuclide for cancer therapy was hampered by several drawbacks including the 1) rapid elimination leading to insufficient therapeutic efficiency, 2) nonspecific distribution resulting in side effects, and 3) inability in treating cancer metastases. There have been reports showing that RIT could induce ICD to produce TAAs, which presented by APCs to CTLs, would trigger specific immunotherapy to cancer metastasis. However, the therapeutic efficacy was restrained by immature DCs and abundant PD-L1 expressed on cancer cells, where PD-L1 would be further promoted by RIT. Hence, there is a great urgent for developing biocompatible scaffolds for long-term tumoral retention of therapeutic radionuclides and meanwhile stimulating immune response. Herein, BC was applied to immobilize ^{131}I-lableld αPD-L1 mAbs specifically in the tumor site as well as stimulate immune response to achieve durable and specific radio-immunotherapy of cancer.

Among ^{131}I-αPD-L1/BC, BC showed 1) satisfactory biocompatibility due to the biogenic derivation, 2) long-term retention of therapeutic agents by the crisscrossed network, as well as 3) immunostimulatory effect to promote DC maturity by LPS. The local injection of ^{131}I-αPD-L1/BC could on only effectively inhibit the primary tumors, but also produce TAAs from ICD to suppress the untreated tumors on the other side. The distal effect on inhibiting tumoral growth was verified in both CT26 and 4 T1 subcutaneous model.

The mechanism for the outstanding therapeutic efficacy was analyzed, showing that after the long-term RIT and ICB of the primary tumors by ^{131}I-αPD-L1/BC, T cells in lymph nodes were polarized to $CD8^+$ CTLs when encountered with DC-presented TAAs. The tumor-specific CTLs then trafficked and infiltrated into the distal tumors and effectively killed cancer cells with the help of TNF-α and IFN-γ cytokines. Furthermore, the enhanced radio-immunotherapy based on ^{131}I-αPD-L1/BC successfully prevented the spontaneous cancer metastasis in the orthotopic breast tumor model, achieving 100% survival rate with steady body weight. Moreover, the histological analysis confirmed the biosafety of ^{131}I-αPD-L1/BC at least during our observation period.

In conclusion, we have designed a BC scaffold to immobilize ^{131}I and αPD-L1 for long-term tumoral retention, achieving safe and efficient therapeutic efficacy in primary, distal and metastases tumors by combining the superiorities of RIT and immunotherapy. We believe that this promising strategy for clinical cancer therapy would inspire more efforts in material design and treatment integration.

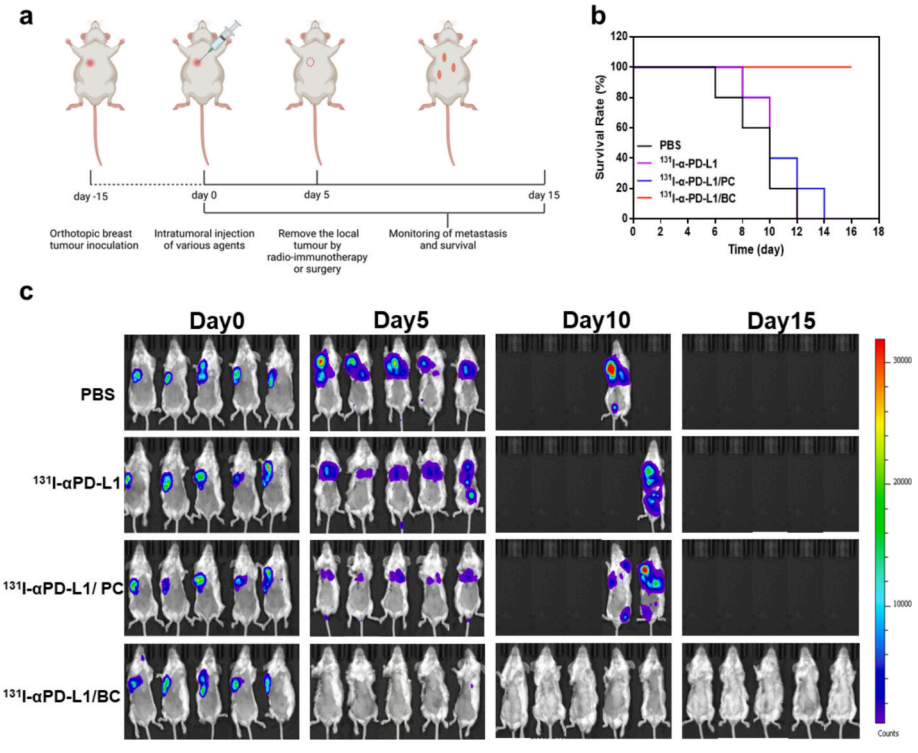

Fig. 7. Radio-immunotherapy of 4 T1 metastasis. **(a)** Schematic illustration of local administration of various agents to inhibit spontaneous tumor metastasis in an orthotopic 4 T1 breast tumor model. **(b)** Survival rate of orthotopic 4 T1 tumor-bearing mice after treating the local tumors (n = 5 per group). **(c)** *In vivo* bioluminescence images to track cancer metastases in different groups of mice after various treatments to eliminate their primary orthotopic tumors. An orthotopic breast tumor model was established by implanting fLuc-4 T1 breast cancer cells into the breast pad of each mouse. After the elimination of local primary tumors by ^{131}I-αPD-L1/BC, radiotherapy and the generated immune responses could effectively inhibit the growth of tumor metastases.

CRediT authorship contribution statement

Zhongyuan Qi: Conceptualization, Investigation, Visualization, Writing – original draft. **Pei Pei:** Methodology, Investigation, Visualization, Writing – original draft. **Yanxiang Zhang:** Investigation, Validation. **Hua Chen:** Investigation. **Sai Yang:** Investigation. **Teng Liu:** Methodology, Resources, Funding acquisition, Writing – review & editing. **Yujuan Zhang:** Methodology, Investigation. **Kai Yang:** Conceptualization, Methodology, Resources, Supervision, Funding acquisition, Writing – review & editing.

Acknowledgments

This work was partially supported by the National Natural Science Foundation of China (31822022, U1932208, 32171382, 32000990), the Natural Science Foundation of Jiangsu Province (BK20190946), and the Project Funded by the Priority Academic Program Development of Jiangsu Higher Education Institutions (PAPD).

Appendix A. Supplementary data

Supplementary data to this article can be found online at https://doi.org/10.1016/j.jconrel.2022.04.029.

References

[1] R.N. Kjellberg, Radiation therapy, Science 176 (4039) (1972) 1071.
[2] G. Delaney, S. Jacob, C. Featherstone, M. Barton, The role of radiotherapy in cancer treatment: estimating optimal utilization from a review of evidence-based clinical guidelines, Cancer 104 (6) (2005) 1129–1137.
[3] G. Dietrich, Radiation injuries caused by radium and radioisotope therapy, Strahlentherapie 114 (1961) 128–134.
[4] P. Pei, T. Liu, W. Shen, Z. Liu, K. Yang, Biomaterial-mediated internal radioisotope therapy, Mater. Horiz. 8 (5) (2021) 1348–1366.
[5] Y. Tao, Y. Sun, K. Shi, P. Pei, F. Ge, K. Yang, T. Liu, Versatile labeling of multiple radionuclides onto a nanoscale metal-organic framework for tumor imaging and radioisotope therapy, Biomater. Sci. 9 (8) (2021) 2947–2954.
[6] R. Nath, L.L. Anderson, G. Luxton, K.A. Weaver, J.F. Williamson, A.S. Meigooni, Dosimetry of interstitial brachytherapy sources: recommendations of the AAPM Radiation Therapy Committee Task Group No. 43. American Association of Physicists in Medicine, Med. Phys. 22 (2) (1995) 209–234.
[7] A. Herskovic, K. Martz, M. Al-Sarraf, L. Leichman, J. Brindle, V. Vaitkevicius, J. Cooper, R. Byhardt, L. Davis, B. Emami, Combined chemotherapy and radiotherapy compared with radiotherapy alone in patients with cancer of the esophagus, N. Engl. J. Med. 326 (24) (1992) 1593–1598.
[8] G. Kroemer, L. Galluzzi, O. Kepp, L. Zitvogel, Immunogenic cell death in cancer therapy, Annu. Rev. Immunol. 31 (2013) 51–72.
[9] D.V. Krysko, A.D. Garg, A. Kaczmarek, O. Krysko, P. Agostinis, P. Vandenabeele, Immunogenic cell death and DAMPs in cancer therapy, Nat. Rev. Cancer 12 (12) (2012) 860–875.
[10] L. Galluzzi, I. Vitale, S. Warren, S. Adjemian, P. Agostinis, A.B. Martinez, T. A. Chan, G. Coukos, S. Demaria, E. Deutsch, D. Draganov, R.L. Edelson, S. C. Formenti, J. Fucikova, L. Gabriele, U.S. Gaipl, S.R. Gameiro, A.D. Garg, E. Golden, J. Han, K.J. Harrington, A. Hemminki, J.W. Hodge, D.M.S. Hossain, T. Illidge, M. Karin, H.L. Kaufman, O. Kepp, G. Kroemer, J.J. Lasarte, S. Loi, M. T. Lotze, G. Manic, T. Merghoub, A.A. Melcher, K.L. Mossman, F. Prosper, O. Rekdal, M. Rescigno, C. Riganti, A. Sistigu, M.J. Smyth, R. Spisek, J. Stagg, B. E. Strauss, D. Tang, K. Tatsuno, S.W. van Gool, P. Vandenabeele, T. Yamazaki, D. Zamarin, L. Zitvogel, A. Cesano, F.M. Marincola, Consensus guidelines for the definition, detection and interpretation of immunogenic cell death, J. Immunother. Cancer 8 (1) (2020).
[11] H.E. Barker, J.T. Paget, A.A. Khan, K.J. Harrington, The tumour microenvironment after radiotherapy: mechanisms of resistance and recurrence, Nat. Rev. Cancer 15 (7) (2015) 409–425.
[12] M.T. Dillon, K.F. Bergerhoff, M. Pedersen, H. Whittock, E. Crespo-Rodriguez, E. C. Patin, A. Pearson, H.G. Smith, J.T.E. Paget, R.R. Patel, S. Foo, G. Bozhanova, C. Ragulan, E. Fontana, K. Desai, A.C. Wilkins, A. Sadanandam, A. Melcher, M. McLaughlin, K.J. Harrington, ATR inhibition potentiates the radiation-induced inflammatory tumor microenvironment, Clin. Cancer Res. 25 (11) (2019) 3392–3403.
[13] M. McLaughlin, E.C. Patin, M. Pedersen, A. Wilkins, M.T. Dillon, A.A. Melcher, K. J. Harrington, Inflammatory microenvironment remodelling by tumour cells after radiotherapy, Nat. Rev. Cancer 20 (4) (2020) 203–217.
[14] D.M. Pardoll, The blockade of immune checkpoints in cancer immunotherapy, Nat. Rev. Cancer 12 (4) (2012) 252–264.
[15] H. Tang, Y. Liang, R.A. Anders, J.M. Taube, X. Qiu, A. Mulgaonkar, X. Liu, S. M. Harrington, J. Guo, Y. Xin, Y. Xiong, K. Nham, W. Silvers, G. Hao, X. Sun, M. Chen, R. Hannan, J. Qiao, H. Dong, H. Peng, Y.X. Fu, PD-L1 on host cells is essential for PD-L1 blockade-mediated tumor regression, J. Clin. Invest. 128 (2) (2018) 580–588.
[16] H. Lin, S. Wei, E.M. Hurt, M.D. Green, L. Zhao, L. Vatan, W. Szeliga, R. Herbst, P. W. Harms, L.A. Fecher, P. Vats, A.M. Chinnaiyan, C.D. Lao, T.S. Lawrence, M. Wicha, J. Hamanishi, M. Mandai, I. Kryczek, W. Zou, Host expression of PD-L1 determines efficacy of PD-L1 pathway blockade-mediated tumor regression, J. Clin. Invest. 128 (2) (2018) 805–815.
[17] F.P. Vendetti, P. Karukonda, D.A. Clump, T. Teo, R. Lalonde, K. Nugent, M. Ballew, B.F. Kiesel, J.H. Beumer, S.N. Sarkar, T.P. Conrads, M.J. O'Connor, R.L. Ferris, P. T. Tran, G.M. Delgoffe, C.J. Bakkenist, ATR kinase inhibitor AZD6738 potentiates CD8+ T cell-dependent antitumor activity following radiation, J. Clin. Invest. 128 (9) (2018) 3926–3940.
[18] A.L. Shergold, R. Millar, R.J.B. Nibbs, Understanding and overcoming the resistance of cancer to PD-1/PD-L1 blockade, Pharmacol. Res. 145 (2019), 104258.
[19] A. Lopez-Soto, S. Gonzalez, A.R. Folgueras, I.F.N. Signaling, I.C.B. Resistance, Time is on tumor's side, Trends Cancer 3 (3) (2017) 161–163.
[20] M. Ruiz de Galarreta, E. Bresnahan, P. Molina-Sanchez, K.E. Lindblad, B. Maier, D. Sia, M. Puigvehi, V. Miguela, M. Casanova-Acebes, M. Dhainaut, C. Villacorta-Martin, A.D. Singhi, A. Moghe, J. von Felden, L. Tal Grinspan, S. Wang, A. O. Kamphorst, S.P. Monga, B.D. Brown, A. Villanueva, J.M. Llovet, M. Merad, A. Lujambio, Beta-catenin activation promotes immune escape and resistance to anti-PD-1 therapy in hepatocellular carcinoma, Cancer Discov. 9 (8) (2019) 1124–1141.
[21] L. Chocarro de Erauso, M. Zuazo, H. Arasanz, A. Bocanegra, C. Hernandez, G. Fernandez, M.J. Garcia-Granda, E. Blanco, R. Vera, G. Kochan, D. Escors, Resistance to PD-L1/PD-1 blockade immunotherapy. A tumor-intrinsic or tumor-extrinsic phenomenon? Front. Pharmacol. 11 (2020) 441.
[22] P. Pei, W.H. Shen, H.L. Zhou, Y.C. Sun, J. Zhong, T. Liu, K. Yang, Radionuclide labeled gold nanoclusters boost effective anti-tumor immunity for augmented radio-immunotherapy of cancer, Nano Today 38 (2021).
[23] C. Tang, X. Wang, H. Soh, S. Seyedin, M.A. Cortez, S. Krishnan, E. Massarelli, D. Hong, A. Naing, A. Diab, D. Gomez, H. Ye, J. Heymach, R. Komaki, J.P. Allison, P. Sharma, J.W. Welsh, Combining radiation and immunotherapy: a new systemic therapy for solid tumors? Cancer Immunol. Res. 2 (9) (2014) 831–838.
[24] R.S. Herbst, G. Giaccone, F. de Marinis, N. Reinmuth, A. Vergnenegre, C.H. Barrios, M. Morise, E. Felip, Z. Andric, S. Geater, M. Ozguroglu, W. Zou, A. Sandler, I. Enquist, K. Komatsubara, Y. Deng, H. Kuriki, X. Wen, M. McCleland, S. Mocci, J. Jassem, D.R. Spigel, Atezolizumab for first-line treatment of PD-L1-selected patients with NSCLC, N. Engl. J. Med. 383 (14) (2020) 1328–1339.
[25] S. Zhao, W. Pan, H. Jiang, R. Zhang, H. Jiang, Z. Liang, H. Hu, Cerenkov luminescence imaging is an effective preclinical tool for assessing colorectal cancer PD-L1 levels in vivo, EJNMMI Res. 10 (1) (2020) 64.
[26] H. Tu, M. Zhu, B. Duan, L. Zhang, Recent progress in high-strength and robust regenerated cellulose materials, Adv. Mater. 33 (28) (2021), e2000682.
[27] A.H. Bhat, I. Khan, M.A. Usmani, R. Umapathi, S.M.Z. Al-Kindy, Cellulose an ageless renewable green nanomaterial for medical applications: an overview of ionic liquids in extraction, separation and dissolution of cellulose, Int. J. Biol. Macromol. 129 (2019) 750–777.
[28] I. Ohad, I.O. Danon, S. Hestrin, Synthesis of cellulose by Acetobacter xylinum. V. Ultrastructure of polymer, J. Cell Biol. 12 (1962) 31–46.
[29] R.E. Cannon, S.M. Anderson, Biogenesis of bacterial cellulose, Crit. Rev. Microbiol. 17 (6) (1991) 435–447.
[30] J. Wang, J. Tavakoli, Y. Tang, Bacterial cellulose production, properties and applications with different culture methods - a review, Carbohydr. Polym. 219 (2019) 63–76.
[31] J. Ye, S. Zheng, Z. Zhang, F. Yang, K. Ma, Y. Feng, J. Zheng, D. Mao, X. Yang, Bacterial cellulose production by Acetobacter xylinum ATCC 23767 using tobacco waste extract as culture medium, Bioresour. Technol. 274 (2019) 518–524.
[32] M. Ul-Islam, S. Khan, M.W. Ullah, J.K. Park, Comparative study of plant and bacterial cellulose pellicles regenerated from dissolved states, Int. J. Biol. Macromol. 137 (2019) 247–252.
[33] R. Naomi, R. Bt Hj Idrus, M.B. Fauzi, Plant- vs. bacterial-derived cellulose for wound healing: a review, Int. J. Environ. Res. Public Health 17 (18) (2020).
[34] X. Wang, C.I. Rousset, H. Hagberg, C. Mallard, Lipopolysaccharide-induced inflammation and perinatal brain injury, Semin. Fetal Neonatal Med. 11 (5) (2006) 343–353.
[35] L.G. Hersoug, P. Moller, S. Loft, Role of microbiota-derived lipopolysaccharide in adipose tissue inflammation, adipocyte size and pyroptosis during obesity, Nutr. Res. Rev. 31 (2) (2018) 153–163.
[36] M. Orecchioni, Y. Ghosheh, A.B. Pramod, K. Ley, Macrophage polarization: different gene signatures in M1(LPS+) vs. classically and M2(LPS-) vs. alternatively activated macrophages, Front. Immunol. 10 (2019) 1084.
[37] N. Kayagaki, M.T. Wong, I.B. Stowe, S.R. Ramani, L.C. Gonzalez, S. Akashi-Takamura, K. Miyake, J. Zhang, W.P. Lee, A. Muszynski, L.S. Forsberg, R. W. Carlson, V.M. Dixit, Noncanonical inflammasome activation by intracellular LPS independent of TLR4, Science 341 (6151) (2013) 1246–1249.
[38] S. Kim, S.G. Yim, A. Chandrasekharan, K.Y. Seong, T.W. Lee, B. Kim, K. Kim, S. Choi, S.Y. Yang, On-site fabrication of injectable (131)I-labeled microgels for local radiotherapy, J. Control. Release 322 (2020) 337–345.
[39] Y. Chao, L. Xu, C. Liang, L. Feng, J. Xu, Z. Dong, L. Tian, X. Yi, K. Yang, Z. Liu, Combined local immunostimulatory radioisotope therapy and systemic immune checkpoint blockade imparts potent antitumour responses, Nat. Biomed. Eng. 2 (8) (2018) 611–621.
[40] M.T.M. Reinders, M.L.J. Smits, C. van Roekel, A. Braat, Holmium-166 microsphere radioembolization of hepatic malignancies, Semin. Nucl. Med. 49 (3) (2019) 237–243.

[41] T. Spyridonidis, N. Papathanasiou, J. Spyridonidis, C. Ntzoumani, D. Spyropoulou, K. Katsanos, D.J. Apostolopoulos, (90)Y-microsphere radioembolization: the method, clinical evidence and perspective, Hell. J. Nucl. Med. 23 (3) (2020) 330–338.
[42] G.W. Aherne, S.L. James, V. Marks, The radioiodination of bleomycin using iodogen, Clin. Chim. Acta 119 (3) (1982) 341–343.
[43] P. Pei, W. Shen, Y. Zhang, Y. Zhang, Z. Qi, H. Zhou, T. Liu, L. Sun, K. Yang, Radioactive nano-oxygen generator enhance anti-tumor radio-immunotherapy by regulating tumor microenvironment and reducing proliferation, Biomaterials 280 (2022), 121326.
[44] F.G. Blanco Parte, S.P. Santoso, C.C. Chou, V. Verma, H.T. Wang, S. Ismadji, K. C. Cheng, Current progress on the production, modification, and applications of bacterial cellulose, Crit. Rev. Biotechnol. 40 (3) (2020) 397–414.
[45] E. Gomez-Ordonez, P. Ruperez, FTIR-ATR spectroscopy as a tool for polysaccharide identification in edible brown and red seaweeds, Food Hydrocoll. 25 (6) (2011) 1514–1520.
[46] X.B. Peng, Q.A. Li, L.N. Ou, L.F. Jiang, K. Zeng, GC-MS, FT-IR analysis of black fungus polysaccharides and its inhibition against skin aging in mice, Int. J. Biol. Macromol. 47 (2) (2010) 304–307.
[47] A. Bosch, D. Serra, C. Prieto, J. Schmitt, D. Naumann, O. Yantorno, Characterization of Bordetella pertussis growing as biofilm by chemical analysis and FT-IR spectroscopy, Appl. Microbiol. Biotechnol. 71 (5) (2006) 736–747.
[48] Y.S. Lee, K.J. Radford, The role of dendritic cells in cancer, Int. Rev. Cell Mol. Biol. 348 (2019) 123–178.
[49] T.A. Patente, M.P. Pinho, A.A. Oliveira, G.C.M. Evangelista, P.C. Bergami-Santos, J. A.M. Barbuto, Human dendritic cells: their heterogeneity and clinical application potential in cancer immunotherapy, Front. Immunol. 9 (2018) 3176.